ANL/RE/CP--75828

DE93 002917

STRENGTH AND RUPTURE-LIFE TRANSITIONS CAUSED BY SECONDARY CARBIDE PRECIPITATION IN HT-9 DURING HIGH-TEMPERATURE LOW-RATE MECHANICAL TESTING*

R.J. DiMelfi, E.E. Gruber, J.M. Kramer, and T.H. Hughes

Argonne National Laboratory

Argonne, IL 60439

Abstract

The martensitic-ferritic alloy HT-9 is slated for long-term use as a fuel-cladding material in the Integral Fast Reactor. Analysis of published high-temperature mechanical property data suggests that secondary carbide precipitation would occur during service life causing substantial strengthening of the as-heat-treated material. Aspects of the kinetics of this precipitation process are extracted from calculations of the back stress necessary to produce the observed strengthening effect under various creep loading conditions. The resulting Arrhenius factor is shown to agree quantitatively with shifts to higher strength of crept material in reference to the intrinsic strength of HT-9. The results of very low constant strain-rate high-temperature tensile tests on as-heat-treated HT-9 that focus on the transition in strength with precipitation will be presented and related to rupture-life.

Introduction

The martensitic-ferritic stainless steel HT-9 is the primary choice for fuel cladding in the Integral Fast Reactor (IFR) under development at Argonne National Laboratory. The alloy would serve in this technology as a structural material in the form of tubes that contain the nuclear fuel, keeping it separate from the flowing liquid-sodium coolant. During service life, the cladding tubes are exposed to high temperature, internal pressure, thermal fluctuations, and fast neutron irradiation. These exposures would contribute ultimately to the failure of the cladding tubes. For reasons both of safety and economy, one would like nuclear fuel elements to have a durable long life. An expected life of five years is not unreasonable. One therefore needs a reliable method of predicting cladding failure under normal and off-normal service conditions. This means not only the prediction of overall life, but of the effects of thermal and mechanical transients that occur at the beginning, middle and end of life, and of the fraction of life that is dissipated by these temporary excursions, as well as the possibility of failure during one of them. The ability to make such predictions from a scientific basis is the subject of this paper. High temperature exposure for long times combined with the atom-displacement damage produced by neutron irradiation make this investigation relevant to the concerns of this symposium on the microstructure of aging materials.

The nominal composition of HT-9 is shown in Table I below. In general

Table I. Nominal Composition of HT-9 (Weight Percent)

Fe	C	Si	Mn	Cr	Ni	Mo	W	V
Bal.	0.20	0.4	0.55	11.5	0.5	1.0	0.5	0.3

it exhibits the desirable properties of good high temperature strength, reasonable corrosion resistance, and excellent resistance to irradiation creep and swelling. When properly heat-treated for service it has the microstructure typical of tempered martensite (Fig. 1). With regard to long time service at high

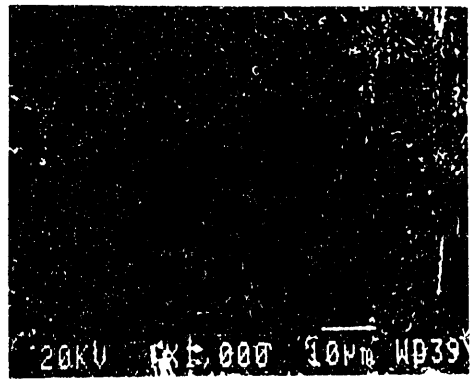

Figure 1: A scanning electron micrograph of an as-heat-treated sample showing the microstructure typical of tempered martensite.

temperatures, this microstructure is inherently unstable. A common reflection of this instability is the coarsening of this structure, upon aging,

* Work supported by the U.S. D.O.E. Technology Support Programs under contract number W-31-109-Eng-38.

accompanied by measurable softening of the material. A less common, though observed [1,2], high-temperature aging phenomenon is the strengthening of this class of alloys via the occurrence of secondary carbide precipitation in ferrite regions formed during coarsening. The nature of this mechanism is such that it is likely to have a greater effect on the creep strength than on the low-temperature mechanical properties [2]. Thus, under the service conditions of interest, the mechanical behavior of austenitized and tempered HT-9 will evolve over time, perhaps going through successive stages of strengthening and softening. These changes, which are reflections of the natural microstructural evolution, will effect the way damage is accumulated at each stage of service life. If one is devising a cumulative damage correlation to be used in a life fraction calculation to predict cladding life, one needs to give consideration to the effects of microstructural changes of this kind. The work described in this paper will help in that process.

Background

Rupture

In investigating the properties of HT-9 for fast reactor service, it was observed that there appeared to be a discrepency between its long-time and short-time high-temperature rupture behavior. This is illustrated in Fig. 2, which is a "stress-rupture" plot of failure

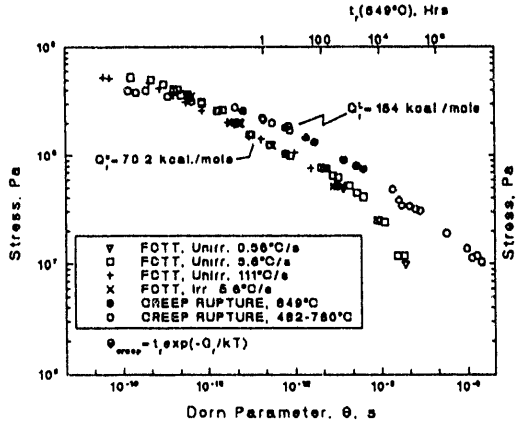

Figure 2: Transient (FCTT [3]) data and creep-rupture data [4] normalized over wide temperature and stress ranges using the Dorn parameter (see text).

data for this alloy. The failure time t_r is normalized by an Arrhenius factor, and the resulting quantity, $t_r \exp(-Q_r/RT) \equiv \theta$, is the Dorn rupture parameter commonly used in this manner to reduce data taken over a wide temperature-time range to a single master curve. In Fig. 2, however, two master curves are shown: one for short-time transients, in which a constant load is maintained on the sample while it is heated at a constant rate (shown) until failure occurs; and another for creep-rupture tests conducted at constant stress and temperature until failure occurs. The short-time transient rupture data [3], reflecting the occurrence of failure over a wide temperature range, were brought into coherence along a single curve by using an activation energy for short-time behavior Q_r^S = 70.17 kcal/mole in the Dorn parameter. We will show later that this is about equal to the activation energy for creep flow, which is also that for self-diffusion in this material (iron in ferrite). A separate master curve associated with the long-time stress-rupture data [5] is also shown in the figure. For the purposes of display this data, taken over a wide range of temperature and time, is normalized in terms of the set of data taken at 650°C (923 K) by multiplying the observed rupture time at each temperature by the factor $\exp[(-Q_r^L/R)(1/T-1/923)]$. This operation brings these data into coherence along a single curve. The activation energy required to do this for long-time behavior is Q_r^L = 154 kcal/mole, a value greater than twice that for creep flow. From this fact, it is clear that the temperature dependence of the rupture time is very different for long-time and short-time tests. These data are included in the Dorn-parameter plot by multiplying the modified rupture time by the factor $\exp(-Q_r^S/923R)$. When this is done, it is seen that this body of stress-rupture data exhibits, for large θ, longer rupture times at a given stress than the transient data, implying that rupture itself is delayed by processes that occur during long-time testing. Since, regardless of test temperature the creep-rupture data are all referenced to the 650°C data set, the rupture times indicated along the top axis are those that would prevail if the long-time tests were all performed at that temperature. In this sense, if the short-time master curve were obeyed, failure for a stress-rupture test at 100 MPa would occur after about eleven hours, whereas the long-time master curve would not indicate failure till after 360 hours at 650°C. Moreover, not only is the temperature dependence of rupture different for the two time regimes, but so is the stress dependence (slope of the Dorn-parameter plot). It is important not just to recognize this dichotomy in rupture behavior, but to realize its effect on life prediction for the conditions of interest. Cumulative damage correlations based on one or the other picture will give very different answers with regard to component life estimates. Even if the two separate approaches agree for a given set of model loading conditions, a slight deviation in practice from those conditions can result in a very incorrect life prediction if the wrong model is chosen for the calculation because of the large difference in stress- and temperature-dependencies in the two regimes. It is important, then, to learn and understand the conditions under which the transition from long-time behavior to short-time behavior occurs in order to develop a reliable model capable of following this transition. Also, one needs to understand the effect that short-time loading scenarios have on overall life, and if indeed such transient loading sequences can themselves cause failure. The work discussed in this paper is aimed at developing a basis for this kind of understanding.

Deformation

In an earlier paper on this subject [5], we proposed a connection between the dichotomous rupture behavior discussed above and a similar discrepency between long-time and short-time flow strength of the material. An analysis of this phenomenon was performed based on published constant-stress creep [6] and constant-rate tensile [7] data on HT-9. The long-time high-temperature creep data appears to exhibit a higher strength than the high-temperature short-time tensile

data for the same heat of material given the same heat-treatment. The concept that secondary carbide precipitation occurs during the longer time creep tests but not the tensile tests was introduced to account for the increase in strength. The connection between this behavior and the rupture behavior discussed above can be illustrated in the schematics shown in Figs. 3a and b. In Fig. 3a, devised with a classic creep test in mind, the creep rate decreases as the material strengthens

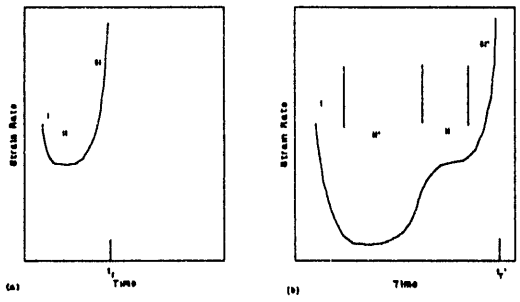

Figure 3: Schematic of creep strain-rate versus time plots for the cases of intrinsic strengthening (a) and extrinsic strengthening, where precipitation delays rupture.

intrinsically via the development of a stronger dislocation structure. Eventually a steady-state structure is achieved and a minimum creep rate (stage II) is sustained until tertiary creep flow mechanisms intercede leading to rupture at t_r. In this scenario, the stress and temperature dependencies of the rupture time have been reasonably related to those of the minimum creep rate [8]. In Fig. 3b, it is suggested that another process, precipitation for example, can cause extrinsic strengthening, producing a minimum creep rate (stage II') that is perhaps lower than the intrinsic minimum in Fig. 3a, and whose duration t_p depends on the kinetics of coarsening. As shown in the figure, this process might be followed by a normal stage II minimum in rate. In this case, the rupture time t_r' is delayed by the precipitation stage, and its temperature dependence is likely to be affected by the kinetics of precipitation. In the earlier paper, we showed this to be the case qualitatively in connection with the rupture-time observations discussed above. We also showed that the stress dependence of rupture for long-time tests could be influenced in the correct way via the introduction of a resistance stress to flow (back stress) produced by the precipitates.

Figure 4 shows a plot of creep [6] and tensile [7] data, in which the flow stress is normalized by the temperature-dependent Young's modulus, and the rate is normalized by an Arrhenius factor with Q_c = 73 kcal/mole. This body of data served as the basis for our analysis [5] of the strengthening effects of precipitation from which we extracted aspects of the kinetics of the precipitation process. The highest-temperature creep data taken over a wide temperature range, shown as filled circles on this graph, are essentially brought into coherence by the normalization implied by the axis labels. The tensile data represented on this plot (open squares) reveal a rate-independent flow stress at high strain-rate and low temperature but show a behavior parallel (in slope) to the creep behavior at low rate and high temperature. The solid line in the figure represents a mathematical correlation that fits the tensile behaviors in the two extremes and provides for a smooth transition between the two. The gap along the

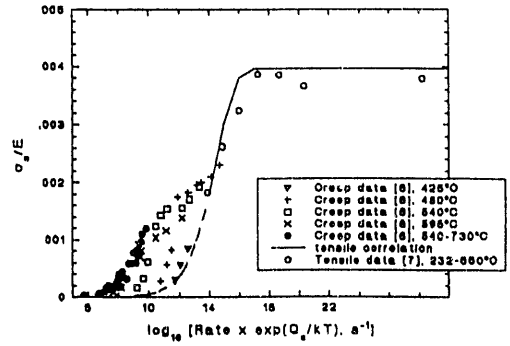

Figure 4: Creep [6] and tensile [7] data compared on a normalized plot. The creeping material shifts to lower rates with increasing temperature.

rate axis between the highest-temperature creep data set and tensile flow behavior in this regime (dashed extension of the tensile correlation) implies that the creeping material is considerably stronger than the tensile-tested material. In addition, creep data obtained at lower temperatures than the highest-temperature data has the same stress dependence (slope) but is situated in intermediate positions depending on test temperature. The lowest temperature data (425°C = 698 K) is essentially in line with the tensile data. The other creep data shift increasingly to lower normalized rate with increasing test temperature. The strength shifts were treated mathematically via the introduction of a back stress in the flow model [2,5]. The back stress represents resistance to flow associated with the Orowan stress for dislocation bowing between precipitates that are assumed to form during high temperature creep flow. Taking the data at 425°C as a base line, the shifts in normalized rate were shown [5] to be reconciled by the factor

$$\exp[(Q_g/k)(1/T - 1/698)], \qquad (1)$$

were T is the absolute temperature of the creep test. The activation temperature, Q_g/k = 25,484 K, was determined from the time and temperature dependencies of the postulated precipitation strengthening process. It is close in magnitude to the activation temperature for diffusion of chromium in ferrite. We used this information to guide aging experiments aimed at producing the postulated precipitates. Figure 5 is a scanning-electron micrograph showing the heat-treated and aged (one day at 740°C) sample. The light spots are chromium-rich carbide precipitates that were not found in the as-heat-treated material (Fig. 1). In the following sections, we briefly describe the analysis that led to these results and that was used to plan low-(constant)rate tensile tests aimed at a further understanding of the strengthening effects that occur during long time service of HT-9. The results of these experiments are examined in the context of the behavior of this alloy over long times at high temperatures.

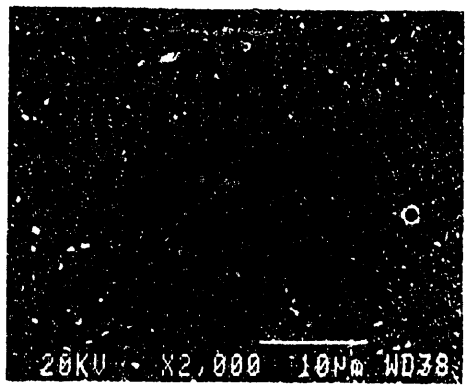

Figure 5: A Scanning electron micrograph of an as-heat-treated sample that was subsequently aged for one day at 740°C. The light spots are chromium-rich carbides.

Analysis

Background

The data in Fig. 4, representing published tensile [7] results, are really the calculated saturation flow stresses σ_s corresponding to the reported yield and ultimate stresses as fit by a Voce-type equation for the flow stress σ of the form:

$$\sigma = \sigma_s - (\sigma_s - \sigma_1) \exp(-\varepsilon_p/\varepsilon_c), \quad (2)$$

where σ_1 is associated with the yield stress ($\varepsilon_p = 0$) and ε_p is the plastic strain. The true stress at the engineering ultimate, σ_u, is defined by Considere's condition,

$$\sigma_u = d\sigma/d\varepsilon_p|_{\varepsilon_{pu}} \quad (3)$$

where ε_{pu} is the reported uniform strain. Equation (1) evaluated at the uniform strain can be solved simultaneously with Eq. (2) to give the saturation stress σ_s and the parameter ε_c, which can be expressed as

$$\varepsilon_c = 0.127 - 3.50 \times 10^{-4}\, T + 2.99 \times 10^{-7}\, T^2, \quad (4)$$

where T is absolute temperature. The saturation stresses for the reported test data are normalized by Young's modulus given by

$$E(T) = 2.12 \times 10^{11}\ \text{Pa}\ (1.144 - 4.856 \times 10^{-4} T). \quad (5)$$

The tensile data for Fig. 4 were obtained at a strain rate of $4 \times 10^{-4}\ s^{-1}$ at temperatures ranging from 25°C to 650°C. The transition from apparent rate independence at low temperature to a creep-like rate dependence discussed above at high temperature was formulated mathematically in our earlier work. Here we concern ourselves primarily with formulating the high-temperature low-rate portion of the tensile behavior, which can be expressed in terms of strain rate as:

$$\dot{\varepsilon}^t = \dot{\varepsilon}^t_o\ (E/\sigma_{so})^n\ (\sigma_s/E)^n \exp(-Q_c/kT), \quad (6)$$

where $\dot{\varepsilon}_o^t = 1.64 \times 10^{14}\ s^{-1}$, $E/\sigma_{so} = 2.525 \times 10^2$, $n = 2.26$, and $Q_c/k = 3.6739 \times 10^4$ K, is the creep activation temperature determined previously [3]. Equation (6) is represented by the dashed line extended from the tensile data. It represents the intrinsic high-temperature flow behavior of HT-9 if precipitation were not to occur during the test.

The highest temperature creep data in Fig. 4 (filled circles) has been fit [5] with an equation similar to Eq. (6), but with the applied stress, replaced by a reduced or effective stress given by

$$\sigma_e = \sigma_s - \sigma_o. \quad (7)$$

Hence,

$$\dot{\varepsilon}^c = \dot{\varepsilon}^t_o\ (E/\sigma_{so})^n\ [(\sigma_s - \sigma_o)/E]^n \exp(-Q_c/kT), \quad (8)$$

We calculate σ_o for each creep data point by determining the value of σ_e that causes Eq. (8) to give the measured creep rate at the test temperature. The creep data displays the same stress exponent as the high-temperature tensile data, i.e. $n = 2.26$. For this condition to be satisfied, it is mathematically necessary that the back stress σ_o be proportional to the applied stress, i.e.

$$\sigma_o = f\sigma_s, \quad (9)$$

where f at a given temperature is a constant less than unity. The resistance to flow represented by σ_o is assumed to come from a fine distribution of carbide precipitates. The mean precipitate spacing is associated with the back stress via the Orowan bowing formula [2]. The proportionality between σ_o and σ_s can be accounted for by imagining that the mean precipitate spacing, under a given set of conditions, is proportional to some measure of the intrinsic dislocation network dimension [9], which itself can be shown to be inversely proportional to the applied stress [2]. As mentioned above, and discussed in detail in the earlier paper [5], an activation energy, $Q_g/k = 25{,}484$ K, associated with the evolution of the precipitate distribution, is determined from an Arrhenius plot of the apparent rate of this process. We used this activation energy to plan static aging experiments that produced precipitates in as-heat-treated HT-9. We also used it to reconcile other apparent strength shifts that occur during lower-temperature creep tests [Eq. (1)], and to plan low-constant-rate tensile experiments aimed at displaying the effects of precipitation, which would further illuminate the transition between long-time and short-time behavior.

Transition Behavior

The other creep data shown in Fig. 4, obtained generally at lower temperatures than the first set, also display the same stress exponent (slope), but only in the low stress range of this data. Also, these data are only partially shifted from the tensile correlation, presumably because precipitation strengthening was limited at these temperatures. The strength shift in this range is temperature dependent and is reconciled by the Arrhenius factor involving Q_g as mentioned above and shown in detail in Ref. 5. However, it is apparent that as the applied stress is increased along these lower-temperature data sets, a level of stress is attained above which the proportionality between the back stress and the applied is no longer maintained. This is manifested by the sudden decrease in slope with increasing stress. These higher stress levels produce ever finer intrinsic microstructures, requiring increasingly dense precipitate distributions to maintain proportionality between σ_o and σ_a. Because of limitations either on constituent availability or precipitation kinetics, the precipitate density can no longer increase to keep up with this proportional relationship. In effect, then, the back stress stays constant in this region. Therefore, further increases in applied stress produce much larger increases in strain rate than would be dictated by a stress exponent of n = 2.26. This causes the appearance in the data of stress plateaus in this transition region. In fact, in this region, the apparent stress exponent n_t from Eq. (8) is given by,

$$n_t = 2.26[\sigma_a/(\sigma_a - \sigma_{oM})], \qquad (10)$$

where σ_{oM} is the maximum value of the back stress achievable at the test temperature. It can be seen from the intermediate temperature creep data in Fig. 4 that the plateau stress level increases with decreasing temperature representative of the finer microstructures accessible at lower temperatures. Equation (10) is such that initially, just at the plateau stress level, n_t can be rather large. Then as stress and rate increase, and the creep data approach the intrinsic flow behavior, n_t approaches the value 2.26 again.

The behavior represented by Eq. (10), and the resulting plateaus, reflect a natural transition at high temperature from flow limited by precipitation strengthening to flow where strength is maintained by the intrinsically developed microstructure. This is an important observation. This region along the normalized rate axis, between the dashed-line extrapolation of the intrinsic flow behavior and the high-temperature creep behavior after precipitation, is precisely the representation in stress/rate space of the transition between long-time and short-time mechanical behavior that we seek. Above the plateau stress at a given temperature, the tests are of such short duration and the flow stress so high that either precipitation does not occur during the test, or if it does, the precipitates present virtually no extrinsic limit to plastic flow. This corresponds to what we term short-time behavior. Below the plateau stress, the precipitation process limits flow, delays rupture and influences its kinetics. The high stress dependence of the rate of flow in this region is the signature of what is happening during any loading scenario at or below the plateau stress, but is only revealed in this region of stress/strain-rate space. The occurrence of this process and its effects cause the observed phenomena that we attribute to long-time behavior. The microstructural transition represented by the plateaus in Fig. 4 occurs at some time during any test performed below the plateau stress. The result is the observed low deformation rate that is obtained in the model by shifting back from the intrinsic rate. The effect on the rupture life depends on the precipitation kinetics and duration of flow at this low rate, as indicated in Fig. 3b. A mechanistic model for the rupture life and its stress and temperature dependencies requires detailed knowledge of the timing of this complex precipitation process. There is no time dependence in Fig. 4, however, so the only manifestation of the transition is for tests performed in the plateau stress region. Nonetheless, this information, if quantified, can be useful in the determination of rupture life because what occurs here reflects the process as it occurs during other tests performed below the plateau.

We next analyze the transition or plateau region in more detail. To do the analysis, we estimate from Fig. 4 the initial plateau stress level from the creep [6] data at three temperatures: 480°, 540° and 595°C. This is the stress level where σ_o stops increasing proportionately with applied stress and remains constant at σ_{oM}. We do not directly know this maximum value of the back stress at each temperature, but our estimates from Fig. 4 of the corresponding applied stress levels are shown in Fig. 6 in an Arrhenius plot. These data are fit rather well by a straight line with

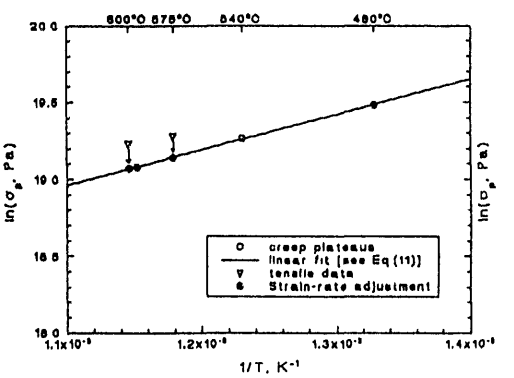

Figure 6: An Arrhenius plot of the initial plateau stresses at three temperatures estimated from the creep data of Fig. 4. Also included on the plot are our tensile data obtained in the plateau region.

a slope of 2291 K shown on the graph, so the initial plateau stress can be described by the equation (from the least squares fit):

$$\sigma_{aP} = 13.26 \exp(2291/T) \text{ Pa}. \qquad (11)$$

This equation can be used to calculate the initial plateau stress at any temperature where a strength shift is observed between the creep and tensile behavior (i.e., T > 425°C). The transition or plateau region is represented by a narrow range in stress. Creep tests performed at applied stresses above this narrow range at a given temperature will display a creep rate corresponding to the intrinsic rate obtained

from tensile data [Eq. (6)]. Below this range in stress, Eqs. (7) and (8) describe the creep rate, which is limited by the back stress produced by secondary carbide precipitation.

We have seen [5] that for creep tests [6] where T > 600°C, the shift along the normalized rate axis between the tensile correlation and the actual creep data (Fig. 4) is about 3.2×10^{-4} s^{-1}. As discussed above, this shift in rate without a change in stress exponent requires proportionality between the back stress and the applied stress, $\sigma_o = f\sigma_a$. The maximum shift at these highest creep temperatures (T > 600° C) corresponds to a value of f = 0.97 [Eqs. (6) and (8)]. The magnitude of rate shifts obtained at lower temperatures are determined using Eq. (1). The value of f necessary to maintain constant stress exponent n = 2.26, after the strength shift, is correspondingly smaller at these temperatures. The fraction f is that value, determined by comparing Eqs. (6) and (8), that produces the reduction in rate calculated using Eq. (1). Clearly, however, in the plateau region of Fig. (4), the stress dependence of the rate [Eq. (10)] is quite different from the value n = 2.26 displayed both above and below the plateau stress level. The temperature dependence in this region is also quite different from the creep activation energy, Q_c, discussed earlier. In fact, it is in these observations that we see quantitatively the connection between the behavior in the plateau region and the effect on the rupture life produced by precipitation occurring during long time creep testing.

We make the following calculations to illustrate the correspondence between what happens in the transition region in stress/strain-rate space, and the process of rupture during "long-time" tests performed at any stress below the plateau stress at a given temperature. We make these calculations at 600°C. At this temperature the plateau stress σ_{aP} = 183 MPa [Eq.(11)], and the corresponding back stress $\sigma_{oM} = 0.97\sigma_{aP}$. If we assume a creep test is run at an applied stress $\sigma_a = 1.09\sigma_{aP}$ = 200 MPa, the test parameters will fall in the transition region of Fig. 4 with $\sigma_a/E = 1.3 \times 10^{-3}$ and a value of about 12 on the normalized rate axis. We have argued that behavior observed under these conditions is a reflection of the reduction in the deformation rate that occurs at any stress below the plateau stress leading to delays in rupture life and an activation energy for rupture considerably larger than that for creep. We can calculate the apparent activation energy for creep flow in the narrow transition range Q_{ct} to make this point:

$$Q_{ct}/R = - d \ln(\dot{\epsilon}^c)/d\,(1/T), \text{ with } \sigma_a/E \text{ constant}, \tag{12}$$

where we use Eq. (8) for $\dot{\epsilon}^c$ with n = 2.26 and Q_c = 73 kcal/mole. Substituting $f\sigma_p$ for σ_{oM}, using Eqs. (1) and (11), and differentiating, we get,

$$Q_{ct}/R = Q_c/R + (2.26)(2291)f/(1.09 - f) - (Q_g/R)(1-f)/(1.09-f) - (2.26)(T^2/E)(dE/dT). \tag{13}$$

This corresponds to an activation energy of about Q_{ct} = 146 kcal/mole which is close to the value of 154 kcal/mole needed to bring long-time rupture data into coherence along a single curve as opposed to the value of about 70 kcal/mole needed to do the same for short-time transient tests, as discussed earlier (Fig. 1). The point is that, for tests conducted below the plateau stress, the rupture time, as an experimental variable, senses the kinetics associated with the reduction in rate produced by precipitation that is displayed in Eq. (13). This is because the microstructural transition occurs during the test and prolongs the test duration. Conversely, the minimum creep rate, as an experimental variable, does not display altered kinetics for tests performed in the region below the plateau stress because the flow mechanism does not change after precipitation. Flow here only requires that the applied stress exceed the back stress to proceed. It is only in tests performed within the narrow plateau region that the strain-rate variable reflects the effects of precipitation on its kinetic law. Within this region, a change in stress or temperature simulates the occurrence of the microstructural transition that causes the shift from flow without precipitation to flow that is limited by it. Above this region, precipitation does not effect the apparent kinetic law associated with either variable. Behavior in this plateau region is important to understanding rupture behavior during long-time high temperature flow and its relation to the behavior during short-time tests. We are, therefore, strongly motivated to perform experiments in this stress/strain-rate range that are specifically aimed at examining these transition phenomena more closely. We describe these experiments and results in the next section.

Mechanical Behavior Experiments

The above models and analyses were developed by comparing published high-temperature creep [6] and tensile [7] data and noting the apparent discrepency in strength exhibited during the two kinds of tests: creep being generally a long-time test and tensile a short-time test. This is analogous to the discrepency observed with regard to rupture life measurements (Fig.1). These behaviors pose a dilemma for those who need to predict mechanical properties and rupture life over a wide range of conditions. After analyzing the data, we believe that the answer to this problem lies in the transition region between deformation at high temperatures and low rates, where precipitation limits flow, and deformation at low temperatures and high rates, where precipitation has either not occurred or does not effect flow or fracture. The pre-existing creep data, while taken in this range, was not focused on this transition behavior and its relation to microstructural change, and took very long times to complete. Published tensile data were taken at rates too high to be in this range at all. We therefore performed tensile tests specifically in this region to further enlighten us with regard to these issues, to see whether these new results would be consistent with model predictions, and to help in further modeling efforts. We believe that very low-(constant)rate tensile tests performed at high-temperatures on as-heat-treated material can best reveal behavior in this transition range as well as the effects of precipitation that occurs during the test. Also, since our model for intrinsic flow behavior was based on the published tensile results taken at higher rates, we performed tests using the same parameters as that data, which are outside the transition region of interest, in order to verify that model. We describe both sets of experiments and examine their results below.

Materials and Procedures

The material used in these tests is from HT-9 rod stock, 0.343" in diameter, supplied by Carpenter Technology (heat #96648). The gauge section of the cylindrical test samples was machined to 0.220" in diameter and 1.25" long. Before testing, the as received material is austenitized for five minutes at 1038°C, "air cooled", then tempered at 760°C for 30 minutes and again "air cooled". All of these treatments are carried out in flowing helium. Constant strain rate tensile tests are performed in strain control on an Instron 8562 Universal Testing machine. Load is applied through an electro-mechanical actuator in this system and is measured to within ± 0.5% accuracy. Strain is measured and controlled to within ± 0.1% with the aid of extensometers clamped to grooves cut in the sample shoulders beyond the gauge section. Post-test measurements at the shoulders indicate that for our tests virtually all of the deformation occurs within the 1.25" gauge section. Constant temperature (± 0.4%) is maintained during testing by the use of a vertically mounted split-tube Instron Model 3117 High-temperature Furnace System and a Model 3120 controller. To limit oxidation during the high-temperature mechanical tests, the sample is contained within a quartz tube through which pure helium is flowed. Test control and data acquisition is fully computer controlled.

Intrinsic Flow Behavior

The tensile data [7] used to fix model parameters in the intrinsic flow regime were all obtained at a strain rate of 4 x 10^{-4} s^{-1} at the temperatures: 25, 232, 400, 450,, 500, 550, 600, and 650°C. Using Eq. (2), the results of these tests were reduced in terms of the steady-state saturation flow stress, σ_s, to be compared with creep data. The correlation for the modulus-normalized saturation stress is plotted against normalized rate in Fig. 7 as the solid line labeled tensile correlation. In order to verify this aspect of the model, we performed tensile tests at a strain rate of 4 x 10^{-4} s^{-1} at 400, 500, and 600°C. These three tests would span the range from rate independent behavior to where the rate dependence of flow becomes almost as high as that for creep flow. The results of these tests are also shown in Fig. 7. It can be seen that they agree within 10% with the correlation developed from the older data from a different heat of material. This agreement adds validity to the model in this flow region, and verifies that the mechanical behavior of HT-9 is somewhat reproducible and consistent.

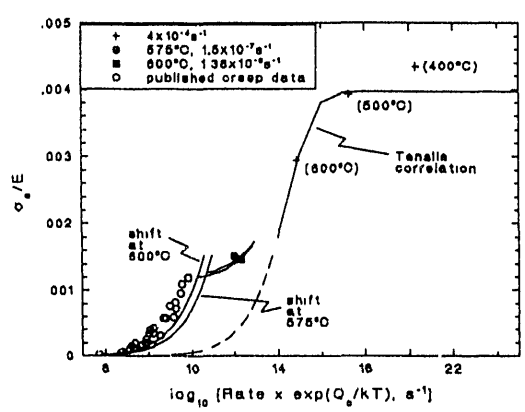

Figure 7: The results of tensile tests performed in the intrinsic flow region (+) and in the transition region at 575° and 600°C shown in comparison with model calculations.

High-Temperature Low-Rate Tensile Tests

The dashed line in Fig.7, as in Fig.4, is the extrapolation of the tensile correlation into the lower-rate/higher-temperature range, where there is no published tensile data. We postulate that this is what flow would be like on this normalized plot if precipitation does not occur during the test. This opinion is verified somewhat by the appearance along this line (Fig. 4) of low-temperature (425°C) creep data. On the other hand, the highest-temperature creep data shown in Fig. 7 display, as before, the shift in strength produced by precipitation. The intermediate temperature creep data, which fall in the transition or plateau region (Fig. 4) discussed above are not shown in this plot. We performed high-temperature low-rate tensile tests whose parameters fall in this range. The idea behind such tests is that the strengthening effects produced by precipitation occurring during the test would be revealed in a constant-rate tensile test in a shorter time than would be required by a creep test. Precipitation strengthening would be reflected in the observed flow strength in the tensile test, while the creep test would require waiting for an ambiguous minimum creep rate to be developed at a given applied stress. Also, the possibility exists that, during a tensile test, flow might be established first at the intrinsic flow stress under these conditions, i.e. as represented by the dashed line in Fig. 7, then undergo a transition to the higher stress associated with precipitation and related to the plateau stress discussed above. This behavior would not be observed if precipitation strengthening were intimately involved with the strain hardening process early in the test. Nonetheless, it will be seen that values of the flow stress (saturation stress) obtained in these constant rate tests performed in the transition region are enlightening with regard to understanding precipitation effects and their relation to the dichotomous deformation and rupture behavior of HT-9.

The first tensile test was performed at 600° C at a rate of 1.38 x 10^{-6} s^{-1}. This corresponds to a value of normalized rate of about 12.3 on the logarithmic-scaled abscissa of Figs. 4 and 7. Because of the high temperature and low rate of this test, a saturation stress was achieved before failure occurred. The test lasted one day and the sample was strained to about 12%. However, the two-tiered flow behavior discussed above, i.e. where flow at the intrinsic level was established first followed by precipitation strengthening, was not apparent in this test. The observed saturation stress was considerably higher than the intrinsic flow stress predicted for these conditions. A second test in this range was performed at 575°C and at 1.5 x 10^{-7} s^{-1}, which corresponds to a value of 12 on the abscissa of Fig. 7. It was hoped that the secondary carbide precipitation process would be suppressed at this temperature and its occurrence

thereby delayed somewhat, and that the longer time test would allow the observation of the effects of microstructural evolution. The postulated two-tiered flow behavior was not observed under these conditions either. The test lasted 10 days and the sample was deformed to about 12% strain again. The saturation flow stress, also achieved before failure, is again considerably greater than the predicted intrinsic flow stress.

While observation of the presupposed two-tiered behavior would have been informative, the measurement of high flow stress levels, indicative of precipitation strengthening during these low-rate tests, is an enlightening effect. The two measured values of the saturation stress are shown in Fig. 7. They are consistent with the plateau stress levels as described in the analysis section, but calculated for the temperatures of these tests. Of course the calculated saturation stress levels had to be adjusted for the rate of the tests also. The plateau stress was defined as the minimum applied stress just at the point where the back stress achieved its maximum level at a given temperature. This occurs at a unique rate. For our tests, performed at a higher rate, a correspondingly higher stress would be given by Eq. (8) with $\sigma_o = \sigma_{oM}$ for comparison with measured values. Conversely, the results of the tests can be extrapolated back to the plateau stress as shown in Fig. 6, where the measured values of saturation stress are shown along with the extrapolated values of the plateau stress calculated using Eq. (7). These latter values fall on the least squares fit obtained from the creep data. Finally, the fact that the two-tiered behavior was not observed even at 575°C can be understood if one imagines that precipitation strengthening consists of two sequential processes. The deformation process has a higher activation energy, Q_c, than that associated with precipitation, Q_g. Therefore, lowering the temperature (to 575°C) would suppress deformation-related strengthening more than it would slow precipitation. This would cause the occurrence of precipitation strengthening even earlier during strain-hardening (at lower strain) than for the test at 600°C. Hence, if the two-tiered flow stress phenomenon was not observed at 600°C, it would be even less likely observed at 575°C. If this view is correct, it would suggest running tests at temperatures higher than 600°C to look for this phenomenon. It also might require performing tests at rates below where the plateau region is observed. This might place the constant-rate tensile experiments in the creep regime, and defeat the purpose of resolving these effects with short-time testing. Higher temperature tests of limited duration are planned to pursue further the possibility of viewing the evolution of precipitation strengthening. Nonetheless, the fact that the saturation stresses for the two tensile tests that were performed in this work agree with creep data in the plateau region, and agree with the model in this region, lends support to the picture presented in this paper.

Discussion and Conclusions

Rupture Correlations

Through analysis and experiment, we have established for HT-9 a connection between behavior in the plateau region in stress/strain-rate space and the dichotomous rupture behavior discussed at the beginning of this paper. Short of a mechanistic rupture model involving detailed knowledge of precipitation kinetics, the information gained from our analysis may be helpful in deciding which rupture correlation should be used under given conditions. Based on our experimental and theoretical findings, it is not unreasonable to suggest as a start that for cases where the applied stress is above the plateau stress, for a given temperature, the short-time rupture correlation prevails. Whereas for cases in which the applied stress is below the plateau stress, one would apply the long-time rupture correlation to predict life. The plateau region represents stress levels where precipitation, if it exists, is losing its influence on flow as stress is increased. Above this level, the test duration is so short that precipitates do not exist, or the flow stress is so high that existing precipitates have no effect. Below the plateau stress, precipitates exist, and their presence severely reduces the flow rate and thereby delays rupture.

The validity of the above suggestion can be examined by comparing rupture data and predictions from the two correlations illustrated in Fig. 1. It should be noted that, because it was developed from thermal transient data, the Dorn parameter θ_s for the short-time correlation was determined by integration over temperature in a way consistent with the usual definition of this parameter:

$$\theta_s = (kT_f^2/Q_r^s\dot{T}) \exp(-Q_r^s/kT_f) . \qquad (14)$$

In Eq.(14), T_f is the failure temperature, and $\dot{T}$ is the heating rate (shown in Fig. 1 for the data). The initial temperature of these tests was 500°C. For a stress of 300 MPa, and a heating rate of 5.6 K/s, the short-time correlation would indicate failure at 650°C in about $t_s = 27$ s, while the long-time correlation would show failure at this temperature and stress to occur in $t_L = 4.5$ s. Hence, at this stress and temperature $t_L < t_s$. Similarly, at a stress of 200 MPa and a rate of 5.6 K/s, the short-time correlation gives failure at 767°C in 47 s, while the long-time correlation indicates failure after only 0.3 s at this temperature and stress. This value of rupture time is still shorter than what the short-time correlation yields for a constant temperature test conducted at 200 MPa and 767°C throughout, namely, $t_s = 5.6$ s. Since the long-time rupture life, t_L, is less than the short-time value, t_s, in all of these results, they appear to offer a contradiction. They imply that rupture is delayed by the precipitation process to yield **shorter** rupture lives as calculated by the long-time correlation. However, in both cases, the applied stresses are above the respective plateau stresses as determined in the analysis section. At 650°C, $\sigma_{sp} = 158$ MPa, and at 767°C, $\sigma_{sp} = 119$ MPa. Therefore, the very phenomena that cause the delay in rupture and the high temperature dependence associated with the long-time correlation, i.e. the occurrences of precipitation and strengthening, are inoperative at the applied stress levels for these tests. Consequently, the predictions of the long-time correlation are invalid in these cases and the predictions of the short-time correlation prevail, as observed. From the other perspective, failure in a stress rupture test conducted at 100 MPa and 650°C occurs at a calculated time of $t_L = 360$ hr according to the long-time correlation and after $t_s = 11$ hr as determine by the short-time correlation for a constant temperature test. Here, no contradiction is implied by the results, i.e. $t_s < t_L$. Since the applied stress is below the plateau stress at this temperature, we suggest that the short-time correlation is inoperative in this case

because rupture is delayed by the effects of precipitation as reflected in the long-time correlation. This expectation has in fact been verified by recent experimental results conducted on IFR fuel pins at this temperature and stress level [10].

All of these results indicate an observed trend that might be thought counter-intuitive or at least non-conservative, i.e. that the correlation that works under a given set of conditions is the one that gives the longer rupture time. However, this is a natural consequence of concepts discussed in this paper. Certain characteristic elements of the long-time correlation, namely strong dependence on stress and temperature, cause this correlation to predict shorter rupture times at high stress and low temperature than the short-time correlation. In the context of our model, these elements are themselves produced by precipitation. However, according to the model, precipitation does not occur or has no effect at high stresses and low temperatures, so the long-time correlation would not be expected to apply under these conditions. Conversely, when precipitation does occur at high temperature and low stress, it acts to delay rupture to longer times than the extrapolated short-time correlation. Consequently, in both test regimes, the model that predicts the longer rupture life prevails. This is not a non-conservative failure prediction strategy, but simply the consequence of the alloy's unstable microstructure and its relation to flow and fracture behavior.

Concluding Remarks

The class of alloys represented by HT-9 is inherently unstable. With regard to its microstructure and mechanical properties, this material ages in high-temperature service. There is evidence that it can both coarsen in the usual sense of martensitic alloys causing a reduction in low temperature strength, and experience secondary carbide precipitation resulting in strengthening at high temperatures. The prediction of failure of HT-9 components during long-time service requires recognition of the microstructural instability of this alloy, its effect on rupture and a method of accounting for it. We have focused here on the strengthening effects produced by secondary carbide precipitation. Our previous analysis [5] of the strength difference displayed during long-time flow versus short-time flow established a link between microstructural evolution and flow behavior in HT-9. Large discrepancies in flow rate between creep and tensile correlations were reconciled by invoking the concept of a back stress associated with the appearance of secondary carbides in the microstructure during creep flow. An Arrhenius factor involving the activation energy associated with this precipitation process accounts for observed rate reductions during creep at intermediate temperatures. We observed, experimentally, the appearance of chromium-rich carbides produced in a manner consistent with this kinetic factor.

During long-time flow, HT-9 goes through a transition over time from what we term intrinsic flow behavior without precipitate-limited deformation to extrinsic behavior, where the appearance of carbides in the microstructure restricts flow and delays rupture. The rupture life, as an experimental variable, exhibits two separate sets of parameters for stress and temperature dependencies: one for short-time failure based on transient test data, and another for long-time failure based on stress-rupture data. The activation energy and stress exponent for the long-time correlation are much greater than those for the short-time correlation. Understanding, mechanistically, just how microstructural change effects the rupture life and the timing of the transition from short-time mode to the long-time mode requires detailed knowledge of a rather complex precipitation process. Conversely, the stress dependence (the exponent, n) and temperature dependence (the activation energy, Q_c) of the strain rate are the same in these two separate regions. However, there is a transition region in stress/strain-rate space, where the restricting influence of precipitation on flow decreases as the stress is increased. The rate increases so sharply with increasing stress in this region, that it is characterized by apparent plateau stress levels that are themselves temperature dependent. This transition region spans a fairly wide range in rate but a narrow range in stress. Above the plateau range, flow exhibits intrinsic behavior, and below it, extrinsic flow prevails. The stress and temperature dependencies in the plateau region are much higher than those above and below it. In fact, quantitative evaluations of the apparent activation energy in this region, obtained from published creep data and from the results of our own low-rate high-temperature tensile tests, yield the same high values displayed by the long-time rupture correlation. This observation suggests that behavior in this transition region in rate behavior mirrors what happens during stress-rupture tests conducted long enough for precipitation to occur and produce a like transition. We use this analogy between the transition in rate space and the transition over time to see whether the former can be used to dictate which correlation is appropriate to predict failure under given loading conditions. Agreement is intriguing, and points the way to future experiments to further delineate the plateau region via the constant low-rate high-temperature tests described in this work. These tests reveal important aspects of high-temperature behavior in shorter times than typical creep tests. It is hoped that information regarding the timing and evolution of precipitation and its effects on deformation and rupture during long-time service will be further uncovered by these shorter-time tests.

References

1. E.A. Little, D.R. Harries, and F.B. Pickering, Ferritic Steels for Fast Reactor Steam Generators, ed. F.B. Pickering and E.A. Little (London, UK: BNES, 1978), 136-144.

2. K.R. Williams, R.S. Fidler, and M.C. Askins, Creep and Fracture of Engineering Materials and Structures, ed. B. Wilshire and D.R.J. Owen, (Swansea, UK: Pineridge Press, 1981), 475-487.

3. N.S. Cannon, F-H Huang, and M.L. Hamilton, Effects Of Radiation on Materials: 14th International Symposium (Vol. II), ed. N.H. Packen, R.E. Stoller, A.S. Kumar (Philadelphia, PA: ASTM-STP 1046, 1991) 729-738.

4. B.A. Chin, Proceedings: Topical Conference on Ferritic Alloys for use in Nuclear Energy Technology, eds.J.W. Davis and D.J. Michel (Warrendale, PA: AIME, 1984), 593-599.

5. R.J. DiMelfi, E.E. Gruber, and J.M. Kramer, Modeling the Deformation of Crystalline Solids, ed. T.C. Lowe, et al., (Warrendale PA: TMS, 1991), 647-664.

6. R.J. Puigh and G.L. Wire, Proceedings: Topical Conference on Ferritic Alloys for use in Nuclear Energy Technology, eds.J.W. Davis and D.J. Michel (Warrendale, PA: AIME, 1984), 601,606

7. T. Lauritzen, W.L. Bell, an S. Vaidyanathan, Proceedings: Topical Conference on Ferritic Alloys for use in Nuclear Energy Technology, eds.J.W. Davis and D.J. Michel (Warrendale, PA: AIME, 1984), 623-630.

8. F.C. Monkman and N.J. Grant, "An Empirical Relationship between Rupture Life and Minimum Creep Rate in Creep-Rupture Tests", Proc. ASTM, 56 (1956) 593-605.

9. J. Friedel, Dislocations, (Oxford, UK: Pergamon, 1964), 220.

10. Yung Y. Liu, private communication with authors, Argonne National Laboratory, 4 September 1992.

DISCLAIMER

END

DATE FILMED

1/15/93